Green Chemistry

PAPER

View Article Online
View Journal | View Issue

Cite this: *Green Chem.*, 2025, **27**, 4385

Shedding light on the path to multifunctional task-specific supported ionic liquids with enhanced catalyst stability and activity†

Sergio Alcalde,[a] Raúl Porcar,[b] Nuria Martín,[a] Francisco G. Cirujano,[a] Belén Altava[a] and Eduardo García-Verdugo *[a]

Received 15th October 2024,
Accepted 17th March 2025

DOI: 10.1039/d4gc05170j

rsc.li/greenchem

This study introduces an approach to developing catalytic systems using multifunctional Task-Specific Support Ionic Liquid-like Phases (TS-SILLPs). These TS-SILLPs leverage the unique properties of ionic liquids (ILs) while addressing traditional challenges such as high production costs and environmental impact. A small-focused library of multifunctional SILLPs can be prepared by employing click chemistry and solid-phase synthesis. The use of thiolactone chemistry and thiol–alkene click reactions facilitates a straightforward method for the post-functionalization of supported ILs, allowing precise customization of their properties for specific catalytic applications. Specifically, in the 1,3-dipolar copper-catalyzed azide–alkyne cycloaddition (CuAAC) reactions, our findings show that these SILLPs can be tuned not only to provide the catalytic species and to stabilize them, enhancing catalyst activity and selectivity, but also to reduce metal leaching, thus providing a greener, more efficient synthesis. Moreover, the incorporation of Rose Bengal as a photosensitizer within the SILLP framework aids in the regeneration of active copper species, demonstrating high stability and reusability of the catalytic system.

Green foundation

1. This study presents a sustainable catalytic system combining task-specific ILs derived from thiolactone with solid supports. The resulting SILLPs stabilize and activate catalytic species, mimicking biological processes and advancing the use of greener, more effective task specific multifunctional IL-based catalysis, highlighting the potential of these materials to create more efficient, targeted, and environmentally friendly catalytic systems.
2. Our system reduced the *E*-factor for Rufinamide synthesis by up to 83% compared to other routes. It offers an efficient, waste-minimizing process with product recovery by simple filtration and catalyst regeneration through light exposure.
3. Future work could focus on biodegradable or renewable polymer supports, adapting a system for flow processes and scaling up while maintaining high yields and minimizing waste in the synthesis of other drugs.

Introduction

Ionic liquids (ILs) are highly valued for their potential to revolutionize catalytic processes due to their unique properties.[1] However, their application is often hindered by several drawbacks, including high production costs, complex separation processes, and concerns about their eco-toxicological impact. To mitigate these challenges, the use of Support Ionic Liquid-like Phases (SILLPs) on advanced materials presents a promising alternative. SILLPs combine the beneficial properties of both ILs and support materials, effectively bypassing some of the limitations associated with traditional ILs.[2] Besides, they exhibit enhanced mechanical stability, making them more durable and suitable for various applications. Their processability and flexibility are improved, and they allow for better dimensional control over their structure. This makes SILLPs more adaptable to different catalytic processes and environmental conditions. However, designing simple yet effective strategies to introduce molecular structural diversity into SILLPs remains a significant challenge. This is particularly crucial for developing task-specific ILs aimed at catalytic purposes. The ability to tailor the molecular structure of SILLPs opens new avenues for creating more efficient, targeted, and environmentally friendly catalytic systems.

In this regard, click chemistry offers a powerful solution for customizing the structure of ILs for specific tasks.[3] This

[a]*Departamento de Química Inorgánica y Orgánica, Universidad Jaume I, Campus del Riu Sec, E-12071 Castellón, Spain. E-mail: cepeda@uji.es*
[b]*Departamento de Química Orgánica y Bio-orgánica, Facultad de Ciencias, Universidad Nacional de Educación a Distancia (UNED), Avda. Esparta. 28232-Las Rozas, Madrid, Spain*

† Electronic supplementary information (ESI) available. See DOI: https://doi.org/10.1039/d4gc05170j

approach is characterized by high-yield and robust synthetic chemistry, capable of being conducted orthogonally in the presence of various functional groups without interference. This versatility is a key advantage, allowing for precise tailoring of the molecular structures of ILs to suit specific requirements. The compatibility of click reactions with a range of functional groups also means that it can be easily integrated into diverse synthetic pathways, making it an ideal tool for developing multifunctional ILs.

Additionally, the use of solid-phase synthesis,[4] particularly with non-soluble polymer-based materials pre-functionalized with appropriate motifs, presents a straightforward and cost-effective method to produce a targeted library of SILLPs. This approach simplifies the process of introducing structural diversity into SILLPs. By leveraging solid-phase synthesis, one can systematically vary the functional groups and architectures of the polymer supports, thereby generating a wide array of SILLPs tailored to specific applications.

Herein, we report the combination of parallel solid-phase synthesis and click chemistry to develop a simple platform of functionalization-supported ILs based on the use of supported task-specific homocysteine thiolactone ILs (Fig. 1). The presence of thiolactone motifs paves the way for the orthogonal post-functionalization of imidazolium salts through its ammonolysis in the presence of an amine (first level of functionalization) generating *in situ* a –SH group (second level of functionalization). The ILs can be further functionalized by the so-called thiol–alkene "click" reaction between –SH groups and an alkene (third level of functionalization). This simple and highly flexible post-modification protocol makes available a large variety of task-specific supported ILs for precise application through manipulation of a reduced number of common simple intermediates, easily available even on a large scale. The multifunctional motifs of the TS-SILLPs can be designed *a priori* to play multiple roles to enhance the catalytic efficiency.

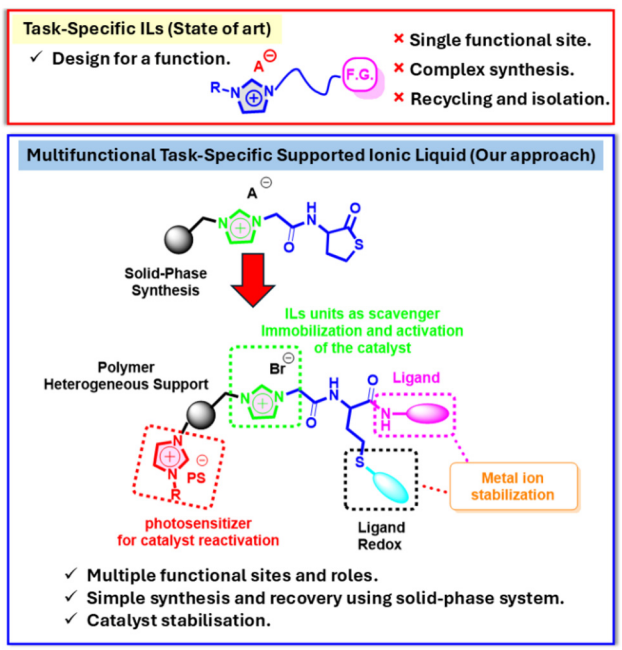

Fig. 1 Approach used in this work for the simple and straightforward preparation and assessment of various supported multifunctionalized task-specific ionic liquids (ILs) designed at a molecular level for specific catalytic roles.

With this idea of designing specific ILs for particular applications, we focus our attention on the development of ILs for 1,3-dipolar copper-catalyzed azide–alkyne cycloaddition (CuAAC), the so-called Huisgen reaction as a potential benchmark catalytic process.[5–7] 1,2,3-Triazole rings formed from azides and terminal acetylenes *via* the Cu(I)-catalyzed cycloaddition reaction are often found to have a variety of biological properties,[8,9] including anti-HIV,[10] antiallergic,[11] antifungal,[12] anticancer,[13] and antibiotic activities.[14] This click reaction often involved the use of Cu(I) salts with a high susceptibility to being oxidized. Different ligands, mainly containing nitrogen, have been evaluated to prevent the Cu(II) from oxidation or disproportionation enhancing the catalytic efficiency in terms of both reaction rate and catalyst stability. Alternatively, the Cu(II) precursors can be used to *in situ* generate the reactive Cu(I) species. Still, they require the presence of an excess suitable reducing agent (*i.e.* sodium ascorbate, hydrazine,[15] tris(2-carboxyethyl)phosphine, *etc.*). The copper-catalyzed 1,3-dipolar cycloaddition, while highly effective, faces a significant challenge due to the presence of toxic, coloured, and expensive copper complexes in the final products.[16] This issue raises concerns about product purity, safety, and cost, especially in applications where these factors are critical, such as pharmaceuticals and fine chemicals. Consequently, various strategies have been developed to facilitate the removal of the copper catalyst from the reaction products including the immobilization of the copper catalyst.[17,18] Another significant challenge is the instability of the Cu(I) oxidation state. Cu(I) is the active form of copper in these reactions. Stabilizing the Cu(I) state is crucial for maintaining the efficiency and longevity of the catalyst.

To address these issues, we design multifunctional TS-SILLPs at the molecular level aiming to retain the catalytic activity of copper while minimizing its drawbacks, thus making the catalyst more efficient, cleaner, and sustainable. We hypothesize that ILs with targeted multifunctionality can lead to several key benefits:

(i) The imidazolium motifs within the IL structure can stabilize copper ions, particularly the Cu(I) state, which is crucial for the catalytic activity in copper-catalyzed reactions like the [3 + 2] cycloaddition to form triazoles. This stabilization is critical in preventing the oxidation of Cu(I) to Cu(II), thereby maintaining the catalyst's effectiveness throughout the reaction. They can also enhance the reaction rate as reported for analogous homogeneous ILs.[19] This effect is likely due to the facilitation of the reaction mechanism, by providing a more favourable environment for the reactants or by enhancing the interaction between the catalyst and the reactants.

(ii) The ionic units can also act as scavengers for charged and nanoparticle species.[20] This is particularly important in

minimizing the leaching of metal, such as copper, into the reaction mixture. By tightly binding or trapping the metal ions or nanoparticles, SILLPs can significantly reduce the contamination of the product with catalyst components. This is an essential advantage ensuring the catalyst's heterogeneous nature and minimizing the possible leaching, especially in reactions where purity is paramount.

(iii) The incorporation of nitrogen-type ligands in ILs mirrors a strategy seen in nature, particularly in proteins, where such ligands play a crucial role in stabilizing metal ions. Nitrogen ligands can effectively stabilize the Cu(I) oxidation state. This is critical because Cu(I) is often the active form of the catalyst in many copper-catalyzed reactions and is susceptible to oxidation to Cu(II) and disproportionation. Nitrogen-type ligands in ILs can mitigate this problem by tightly coordinating with the copper ions, protecting them from reactions that would otherwise lead to their degradation. By stabilizing the copper species, these ligands not only extend the life of the catalyst but can also improve the overall efficiency of the catalytic process. This can lead to higher yields, better selectivity, and the possibility of conducting reactions under milder conditions.[21]

(iv) Inspired by natural systems the presence of free thiol groups in the IL can play an important role indeed in different enzymes, the cysteine residues are the binding sites for copper homeostasis, which is known to be involved in two human disorders of copper transport. It is believed to reduce Cu(II) to Cu(I) while simultaneously oxidizing thiol functions to disulfides.[22] Thiol groups undergo oxidation in the presence of molecular oxygen, a process often catalyzed by transition metal ions like iron or copper. Insights into this mechanism, particularly focusing on the copper-catalyzed auto-oxidation of cysteine,[22] identify the cuprous biscysteine complex (RS–CuI–SR) as the key catalytic species involved in this oxidation process.[23] By incorporating these biological principles into the design of ILs, particularly those featuring free thiol groups and appropriate nitrogen-based ligands, it is possible to develop more effective and stable copper catalysts.[24,25]

(v) The presence of ILs can allow the immobilization and activation of a photosensitizer as a potential co-catalyst to facilitate the recovery of Cu active species. Copper is known for its ability to easily transition between its oxidation states, represented by the reaction $2Cu^{+} \leftrightarrow Cu^{2+} + Cu$. The equilibrium between these two states is quite dynamic and can shift in either direction based on the specific conditions applied. By incorporating a photosensitizer, singlet oxygen ($^1O_2$) can be transformed into various reactive oxygen species (ROS) including superoxide ($O_2^{\bullet -}$), hydrogen peroxide (H_2O_2), and the hydroxyl radical ($OH^{\bullet}$), closely emulating the mechanism of copper-containing oxidases. These enzymes operate *via* cyclic transitions between copper oxidation states, consistently engaging dioxygen. Employing a photosensitizer immobilized into the SILLPs, such as Rose of Bengal, can facilitate the reactivation of the copper species through a straightforward redox reaction in the presence of oxygen, effectively preventing catalyst deactivation.

The methodology described in this report enables the swift and straightforward preparation and assessment of various supported multifunctionalized ionic liquids (ILs) designed at the molecular level for a specific catalytic role. By fine-tuning the structure of ILs, it is possible to effectively adjust their catalytic behaviour of both activity and stability.

Results and discussion

Synthesis of solid-phased task-specific supported IL library

The initial preparation of a small-focus library of task-specific supported ILs was easily carried out as shown in Scheme 1. The direct reaction of the imidazole with chloromethylated polystyrene–divinylbenzene (PS–DVB, macroporous resin, 4.5 meq of Cl per g) polymer provided the corresponding supported imidazole **2**. The alkylation of this supported imidazole with the 2-bromoacetamide of the amino-homocysteine thiolactone **3** in DMF afforded the corresponding immobilized task-specific ILs (**TS-SILLP-4**). In all cases, the reactions could be easily followed using FT-IR. In general, FT-IR spectra of **2** showed the appearance of a new band at *ca.* 1484 cm^{-1} and 1440 cm^{-1} corresponding to the C=C/C=N stretching bands of the imidazole group as well as the disappearance of the C–Cl band at 1263 cm^{-1} and the one at 673 cm^{-1}. The further functionalization of resin **2** can be assessed by the appearance in **TS-SILLP-4** of a broad band in the region 1650–1720 cm^{-1} associated with the C=O stretching of both thiolactone and

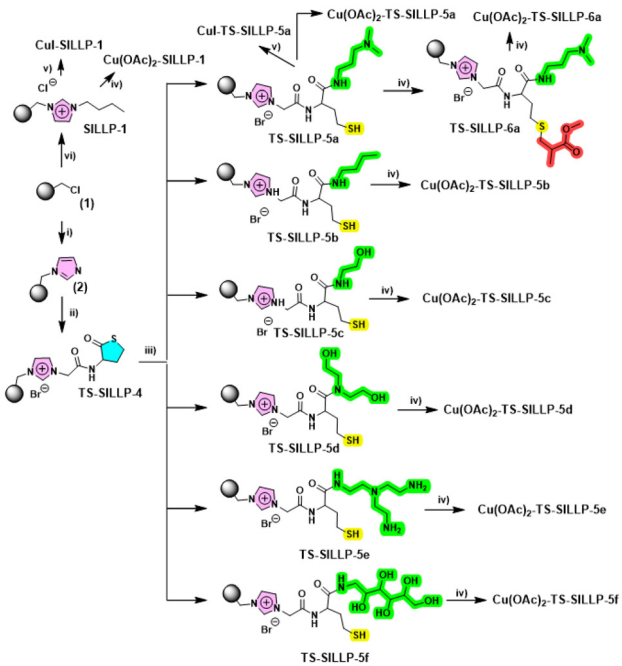

Scheme 1 Synthetic strategy of solid-phased task-specific supported IL library under the following conditions: (i) Merrifield resin **1**, imidazole, DMF, 80 °C, 24 hours; (ii) imidazole polymer **2**, *N*-(2-bromoacetyl)-D,L-homocysteine thiolactone, DMF, 75 °C, 24 hours; (iii) **TS-SILLP-4**, RNH_2, DMF, r.t., 24 hours; (iv) **SILLP-1** or **TS-SILLP-5a-f**, $Cu(AcO)_2{\cdot}H_2O$, DMF, r.t., 24 hours; (v) **SILLP-1** or **TS-SILLP-5a**, CuI, DMF, r.t., 24 hours; (vi) **TS-SILLP-5a**, methyl acrylate, DMF, 70 °C, 24 hours; (vii) Merrifield resin **1**, 1-butylimidazole, DMF, 80 °C, 24 hours.

amide carbonyl groups. Polymer **TS-SILLP-4** also showed a peak at 1554 cm^{-1} corresponding to the C=C/C=N of the imidazolium ring and an intense peak at 920 cm^{-1} assignable to the C–S stretching of the thiolactone ring (Fig. S1†).

Those facts together with the elemental analysis confirm that the grafting of the homocysteine thiolactone moieties took place leading to a support IL with a loading of 1.79 mmol of IL per g of polymer. The post-functionalization of **TS-SILLP-4** with six different amines was performed by suspending the polymer in each corresponding amine, using DMF as a solvent at 60 °C for 20 hours. The process led to several notable chemical changes regardless of the type of amine used. Firstly, there was a disappearance of the spectral shoulder at 1715 cm^{-1}, a feature typically linked with the C=O stretching in thiolactone groups (Fig. S1†). This was accompanied by a shift of the amide C=O stretching peak from 1683 and 1662 cm^{-1} to lower wavenumbers (1678 and 1658 cm^{-1}, Fig. S1†) associated with the ring opening and the formation of C=O of newly obtained amide.

Additionally, the characteristic peak at 910 cm^{-1}, associated with the C–S bonds in thiolactone, was no longer observed. These changes suggest the complete aminolysis of the thiolactone groups. The successful opening of the thiolactone rings was further confirmed by a positive Ellman test, indicative of the presence of –SH groups. In this way, six different task-specific SILLPs (**TS-SILLP-5a-f**) baring free thiol and other functional groups were obtained. In the case of the **TS-SILLP-5a**, the thiol group was further converted into a thioether leading to resin **TS-SILLP-6a**. This was achieved through a straightforward thiol-Michael addition click reaction with methyl methacrylate. The successful synthesis of the thioester was confirmed by a negative Ellman test, indicating the absence of free –SH groups, which would be expected after their conversion into thioethers and by the appearance of a new peak at 1729 cm^{-1} in the ATR-FTIR spectrum (Fig. S1†). This peak is assignable to the C=O stretching vibration of the newly formed ester group.

Catalytic screening of the focus task-specific supported IL library. The cycloaddition between benzyl azide (**7a**) and phenylacetylene (**8b**) as a benchmark reaction was conducted using a library of TS-SILLPs. Both Cu(I) and Cu(II) ions were tested as catalysts using CuI and $Cu(OAc)_2$ salts as the copper source. The supported copper catalysts were prepared by suspending the corresponding supported ILs in a copper salt solution.

The polymer-metal loading achieved is reported in Table 1 which also summarizes the results obtained for the initial screening in the model reaction between **7a** and **8a**. The catalyst **$Cu(OAc)_2$-TS-SILLP-5a** yielded the desired product with excellent efficiency with a 92% yield (Table 1, entry 1). In contrast, **CuI-TS-SILLP-5a** resulted in a slightly lower yield of 77% (Table 1, entry 2). This contrasted with the results for **SILLP-1** without additional functional groups, where **$Cu(OAc)_2$-SILLP-1** was inactive and **CuI-SILLP-1**, although active, showed low activity 37% yield (Table 1, entries 3 and 4). It should be mentioned that other Cu(II) salts (*i.e.* $CuBr_2$ and CuI_2) when immobilized in the **TS-SILLP-5a** did not show any activity. The efficiency of $Cu(OAc)_2$ *vs.* other sources of Cu can be explained by the presence of a more basic anion favouring the promotion of thiolate from the –SH allowing complexation and copper reduction.[26] $Cu(OAc)_2$ can also catalyze, in the presence of alkyne, the formation of Cu(I) by Eglinton oxidative homocoupling.[27]

The substitution of the amide in TS-SILLPs was also evaluated. The polymers derived from butylamine, ethanolamine and diethanolamine (**TS-SILLP-5b-d**) led, respectively, to

Table 1 Evaluation of the immobilized copper TS-SILLPs in the reaction between **7a** and **8a** [a]

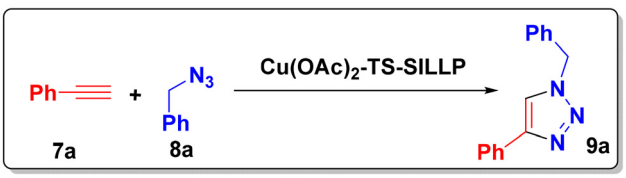

Entry	Copper SILLPs	meq of IL per g [b]	Copper loading,[d] mmol Cu per g	Yield[e] (%)
1	**$Cu(OAc)_2$-TS-SILLP-5a**	1.20	0.50	92
2	**CuI-TS-SILLP-5a**	1.20	1.12	77
3	**$Cu(OAc)_2$-SILLP-1**	1.27[c]	0.65	1
4	**CuI-SILLP-1**	1.27[c]	1.07	37
5	**$Cu(OAc)_2$-TS-SILLP-6a**	1.22	0.41	91
6	**$Cu(OAc)_2$-TS-SILLP-5b**	1.16	0.46	83
7	**$Cu(OAc)_2$-TS-SILLP-5c**	1.21	0.47	84
8	**$Cu(OAc)_2$-TS-SILLP-5d**	1.19	0.47	85
9	**$Cu(OAc)_2$-TS-SILLP-5e**	1.14	0.27	5
10	**$Cu(OAc)_2$-TS-SILLP-5f**	1.21	0.13	11

[a] 0.2 M azide : alkyne (1 : 1) in acetonitrile, 1.5% mol copper catalyst, 4 hours, 70 °C. [b] Calculated by elemental analysis based on S%. [c] Calculated by elemental analysis based on N%. [d] Calculated by ICP-MS after acid hydrolysis of 50 mg SILLP in 10 mL of HNO_3 : HCl (1 : 4), 4 hours, 100 °C. [e] Calculated by HPLC.

slightly lower yields of 83%, 84% and 85% (Table 1, entries 6–8) than the polymer **TS-SILLP-5a**. However, the system obtained with tris(2-aminoethyl)amine (**TS-SILLP-5e**) and methylglucamine (**TS-SILLP-5f**) were almost inactive for the reaction with a yield of 5% and 11%, respectively (Table 1, entries 9 and 10). Finally, in the case of **Cu(OAc)$_2$-TS-SILLP-6a**, where the thiol group is transformed into thioether the system provides similar activity to **TS-SILLP-5a** (91%, Table 1, entry 5).

After identifying **Cu(OAc)$_2$-TS-SILLP-5a** as the most active catalyst, its loading effect was investigated. The initial molar loading of 1.5% based on copper content was decreased to 0.0178% and then further reduced to 0.0004%. This reduction in catalyst loading led to yields of 79% and 38%, respectively (Table S1†). These outcomes highlight the high activity of the copper-supported species. The impact of solvent choice on the reaction was also assessed, comparing the traditional organic solvent dichloromethane (CH_2Cl_2) with greener alternatives such as dimethyl carbonate (DMC) and methyl-THF (Me-THF) (Table S2†). It was observed that the use of CH_2Cl_2 and DMC significantly diminished the reaction yields, achieving only 34% and 35% respectively. In contrast, Me-THF demonstrated comparable efficiency to acetonitrile, with a yield of 88%.

All these results highlight the significant non-innocent nature of the functional groups introduced in **TS-SILLP**, particularly alkylamine ligands and SH groups, in stabilizing copper complexes. The relative stability of Cu^+ and Cu^{2+} complexes depends on the nature of their ligand, and the $2Cu^+ \rightarrow Cu^{2+} + Cu$ equilibrium can shift readily in either direction, depending on reaction conditions. Cu^{2+} prefers binding with intermediate ligands, such as *N*-alkyl groups and imidazolium units. The Cu^+, being a soft acid, forms stronger bonds with soft ligands like SH. Copper, depending on the reaction conditions and the structure of the SILLP, can pass readily from one oxidation state to another, providing favourable conditions for its compounds to execute their redox functions. The higher efficiency of **Cu(OAc)$_2$-TS-SILLP-5a** over **Cu(OAc)$_2$-SILLP-1** can be attributed to the *in situ* generation of Cu(I) from Cu(II) salt, facilitated by free thiol groups—a process not feasible with **Cu(OAc)$_2$-SILLP-1**. This is evidenced by the colour change from blue/green, indicative of Cu(II), to brow-yellow (Cu(I)) (Fig. S2D†). The lower activity of **CuI-TS-SILLP-5a** in comparison with the Cu(II) catalyst is likely due to the unstable nature of Cu(I). The improvement in the activity of **CuI-TS-SILLP-5a** over **CuI-SILLP-1** can be attributed to the stabilization of Cu(I) through the multifunctional **TS-SILLP-5a** by the imidazolium, alkylamine ligands and SH groups.

The scope of the more effective catalyst (**Cu(OAc)$_2$-TS-SILLP-5a**) was evaluated for the synthesis of seven 1,2,3-triazoles with structural diversity (Fig. 2A). In general, the catalyst effectively yielded the targeted products. The lower reactivity azides **8d** and **8f** resulted in reduced yields under standard conditions. The efficiency of the catalyst was further demonstrated in the synthesis of the antiepileptic drug rufinamide (**9g**), achieving a remarkable yield of 81%.

Notably, the comparison of the kinetic profile of the immobilized to homogeneous systems, which rely exclusively on $Cu(OAc)_2$, revealed significant differences in terms of activity, as illustrated in Fig. 2B. The analysis reveals a significantly reduced reaction rate in the homogeneous systems compared to the systems utilizing copper immobilized on the multifunctional supported ionic liquid phase. This outcome highlights the essential role of the multifunctional groups within the TS-SILLPs. These groups serve a dual purpose: they not only stabilize the active copper species but also greatly increase the catalytic activity, demonstrating a marked improvement in efficiency. A similar trend, although less pronounced, has been also observed for the model reaction between **7a** and **8a** (Fig. S3†).

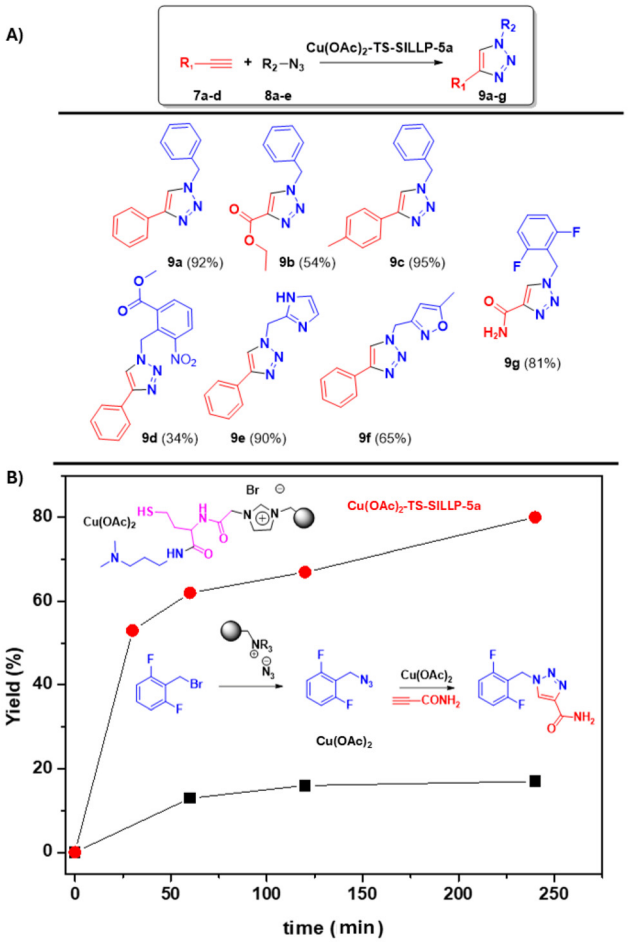

Fig. 2 (A) Scope of the catalyst **Cu(OAc)$_2$-TS-SILLP-5a** for different alkynes and azides. (B) Yield of Rufinamide (**9g**) *vs.* time for immobilized **Cu(OAc)$_2$-TS-SILLP-5a** and $Cu(OAc)_2$ as a homogeneous catalyst (reaction conditions: 0.2 M azide : alkyne (1 : 1) in acetonitrile, 1.5% mol copper catalyst, 70 °C).

Heterogeneous nature and catalyst stability

As mentioned above one of the problems related to some immobilized catalytic systems is the leaching of copper from the support to the solution during the reaction. To evaluate the heterogeneous nature of **TS-SILLP-5a** a hot filtration test was performed. The reaction was allowed to proceed in the

presence of the catalyst for 20 minutes and the catalyst was filtered off and the progress of the reaction was then monitored for an additional four hours. The absence of the catalyst ceased the progression of the reaction. In contrast, a controlled reaction with the catalyst present reached a 91% yield (Fig. S3†).

These results indicate the heterogeneous nature of the active catalytic species, which can be attributed to the scavenging ability of both the excess of imidazolium units and the additional functional groups (*e.g.*, NR_3 and SH), effectively capturing copper species. To validate this, the model reaction was conducted using **CuI-SILLP-1** both in the absence and presence of excess **SILLP-1** and **TS-SILLP-5a** (Fig. S3B–D†). The observed decrease in catalytic activity when excess SILLPs and SILLP-5a were present, combined with the cessation of the reaction after catalyst removal in the hot filtration test, provides strong evidence that both the imidazolium units and functional groups play a crucial role in capturing leached copper species.

Another key feature of an immobilized catalyst is its ability for recovery and reuse. Thus, we evaluated the recyclability of **TS-SILLP-5a** in consecutive cycles of the model reaction (Fig. 3A). Although the catalyst did not show any significant loss of catalytic activity during the initial three cycles after the 4th cycle slight deactivation was observed which was quite significant for the fifth cycle. It should be noted that the colour of the catalyst changed during the reuses from a blue colour from the pristine catalyst to green until (after the 1st cycle) becoming brown after the 5th cycle (Fig. 3B). Low oxidation states of copper (Cu(0) or Cu(I)) are evidenced by the brownish colour of the materials, this suggests that the valence state of copper had changed going from Cu(II) to active Cu(I) until finally reaching the formation of either CuNPs or CuO as low active species.

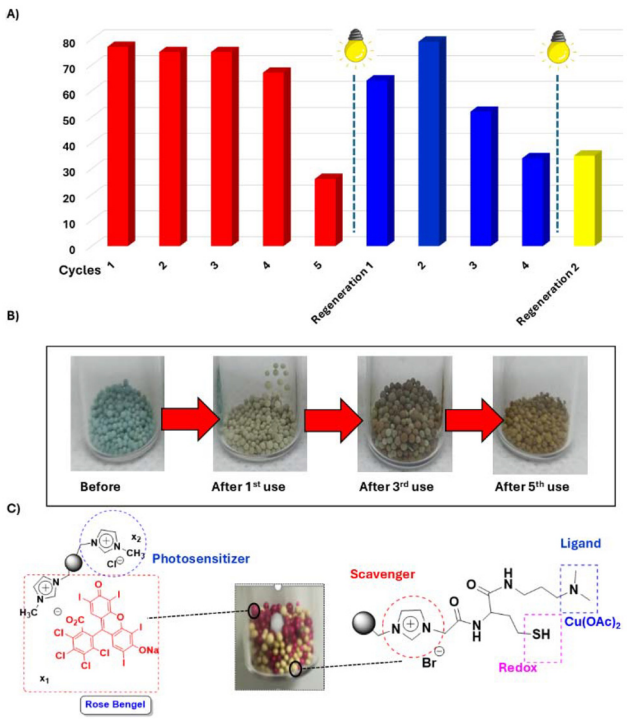

Fig. 3 (A) Reuse and reactivation of **Cu(OAc)$_2$-TS-SILLP-5a** for the reaction between **7a** and **8b**. Red: recycling of **Cu(OAc)$_2$-TS-SILLP-5a** under standard conditions. Blue: reuse of the catalyst **Cu(OAc)$_2$-TS-SILLP-5a** after five uses in a cocktail formed by **Cu(OAc)$_2$-TS-SILLP-5a** and **RB-SILLP-1** (3.92×10^{-2} μmol RB per g loading, 100 mg of the mixture 1 : 1 by weight). 0.2 M azide : alkyne (1 : 1) in acetonitrile, 1.5% mol copper catalyst, 4 hours, 70 °C. (B) Picture of **Cu(OAc)$_2$-TS-SILLP-5a** after different reaction cycles. (C) Picture of a cocktail of **Cu(OAc)$_2$-TS-SILLP-5a** (green-yellowish beads) and **RB-SILLP-1** (red beads) after regeneration.

Looking at a possible strategy to recover the activity of the copper catalyst after five uses, we envisioned integrating **Cu(OAc)$_2$-TS-SILLP-5a** with a photosensitizer, specifically Rose Bengal. The inclusion of the photocatalyst, under aerobic conditions, is hypothesized to facilitate the oxidation of Cu(I) and Cu(0) to Cu(II), thereby sustaining the catalytic process as Cu(II) species can be reduced back to active Cu(I) by the action of free thiols of TS-SILLP.[28] Thus, a cocktail mixture containing the spent catalyst **Cu(OAc)$_2$-TS-SILLP-5a** after five reaction cycles and Rose Bengal, anchored on **SILLP-1** with a loading of 3.92×10^{-2} μmol RB per g of polymer, was prepared.[29] This mixture, suspended in acetonitrile, was subjected to light irradiation at a wavelength of 365 nm in the presence of oxygen. After irradiation, the solvent was filter-off and the polymer cocktail dried before exposing it to a new reaction cycle. The regenerated system demonstrated its capability to catalyze the formation of **9a**, achieving a 64% yield, suggesting the reactivation of the catalyst.

Encouraged by these findings, the system underwent three additional reaction cycles. The first reuse of the cocktail led to a 79% yield, though a decrease in efficiency was observed in the following cycles, with yields of 52% and 34% for the third and fourth cycles, respectively. Following this, a second regeneration attempt was assayed. Unfortunately, this effort failed to restore the catalytic efficiency of the cocktail providing only a moderate yield of 34% yield.

It should be noted that although **Cu(OAc)$_2$-TS-SILLP-6a** initially demonstrated good catalytic activity during the screening process (entry 5, Table 1), a significant decline in catalytic performance was observed after the first cycle (yield of **9a** after the second cycle: 57%; after the third cycle: 18%). Moreover, attempts to regenerate the catalytic system using a catalytic cocktail with **RB-SILLP-1** were unsuccessful, yielding only 25% after regeneration. These results strongly suggest that thiol bonds play a critical role in maintaining the catalytic performance over multiple cycles.

Taking into account these results, a multifunctional system was conceptualized where **Cu(OAc)$_2$-TS-SILLP-5a** was modified further with Rose of Bengal with a loading of 3.92×10^{-2} μmol RB per g of polymer by partial counter ion exchange of the chloride imidazolium units. This system combines the source of copper active species with the photosensitizer for catalyst regeneration. We design, for this system, a specific reaction regeneration protocol. This protocol entails conducting the model reaction under standard conditions (24 hours, 70 °C)

using 0.7% mol of copper catalyst. Following the reaction, the mixture is filtered and washed with ACN, and the catalyst is then subjected to a regeneration cycle. This involves resuspending the supported system in ACN and exposing it to light at a wavelength of 365 nm in the presence of oxygen at room temperature for 1 hour.

According to this reaction regeneration protocol, the catalytic systems were reused without showing any sign of deactivation across ten consecutive cycles. The 11th reaction cycle was carried out only at 4 hours leading to a similar activity to the fresh catalyst under the same conditions (blue bar in Fig. 4). These results highlight that the system is not only reusable in consecutive cycles, but also does not suffer from any potential deactivation. The system can be used for at least during 15th consecutive cycles demonstrating a very high level of stability.

Insights into the catalytic/regeneration cycle

Based on the experimental data gathered and previously published findings regarding the mechanism of copper-based reactions, we put forward a reaction/regeneration mechanism as illustrated in Fig. 5. This mechanism entails the conversion of Cu(II) to Cu(I) species through reduction [2RS$^-$ + 2Cu(II) → RSSR + 2Cu(I)], analogous to the action of cysteine residues in proteins.[22–25] The biomimetic thiol groups present in TS-SILLPs can reduce Cu(II) to Cu(I), while concurrently oxidizing the thiol groups to disulfides (TS-SILLPL–S–S–TS-SILLPL) in a redox reaction that is both facile and thermodynamically favorable.[30] This process of Cu–thiol autoreduction produces

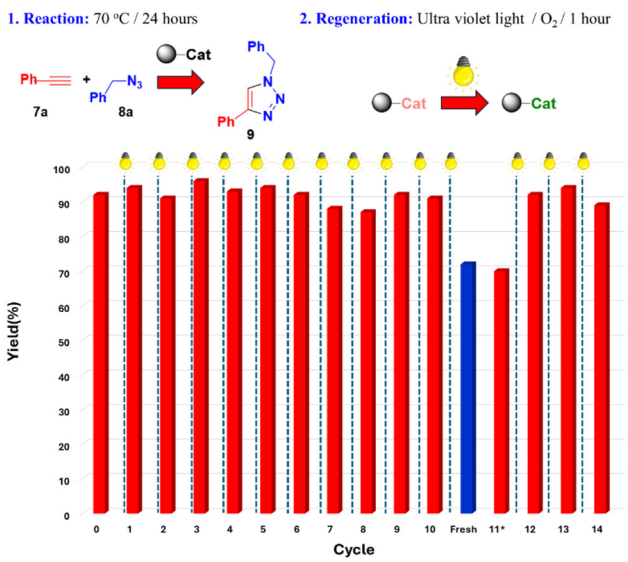

Fig. 4 Reuse and reactivation of multifunctional systems based on **RB-Cu(OAc)$_2$-TS-SILLP-5a** for the reaction between **7a** and **8b**. 0.2 M azide : alkyne (1 : 1) in acetonitrile, 0.7% mol copper catalyst, 24 hours and 70 °C. Blue bar: result obtained for the fresh **Cu(OAc)$_2$-TS-SILLP-5a** at 4 hours and 70 °C. * 11th reuse at 4 hours and 70 °C performed after reactivation.

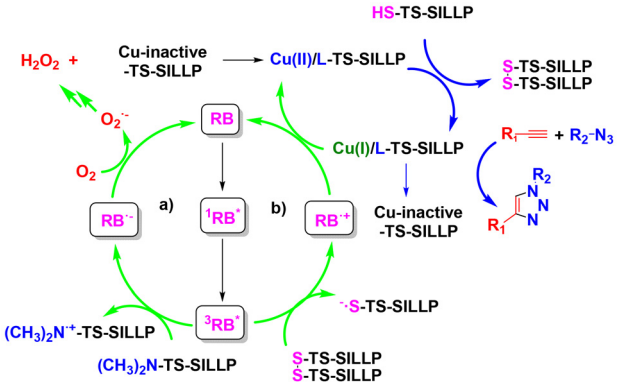

Fig. 5 Proposed mechanism for the reaction and regeneration of the multifunctional task-specific supported ionic liquid-like phases during the click reaction. Blue arrows: reaction pathway. Green arrows: regeneration pathway by two potential pathways either *via* reductive quenching or oxidative quenching as illustrated in cycle (a) and cycle (b).

Cu(I), the active species necessary for the azide–alkyne cycloaddition reaction, as demonstrated in previous studies.[24,25] It is also worth noting that the acetate ions from Cu(OAc)$_2$ might contribute to the formation of Cu(I) through Eglinton oxidative homocoupling. The transitions in the oxidation state of copper are visually observable, as the initial color of the immobilized Cu(OAc)$_2$ changes through cycles of use from blue to green, and finally to yellowish-brown, as seen in Fig. 3B.

The UV-Vis diffuse reflectance spectra of the catalyst as freshly prepared (Fig. S2A and B†) exhibited two broad bands, one spanning 250–550 nm and the other from 550 to 1250 nm. The breadth of these bands suggests the presence of various copper complexes in equilibrium with different functional sites on the catalyst. Notably, the second band for **CuI-SILLP-1** is shifted to a higher wavelength, centered at 780 nm, whereas for **Cu(OAc)$_2$-TS-SILLP-5a**, the maximum is observed at 660 nm. These shifts can be attributed to the differing oxidation states of copper and the distinct ligand → Cu charge transfers, which are influenced by the additional functional groups present in **TS-SILLP-5a**. After the reaction, in the spent catalyst, this band exhibits a decrease in intensity and a shift to a higher wavelength, which can be ascribed to the redox process 2RS$^-$ + 2Cu(II) → RSSR + 2Cu(I), indicating changes in the copper species during the catalytic cycle.

The influence of SH groups in reducing Cu(II) was further corroborated by X-ray photoelectron spectroscopy (XPS) analysis focusing on the Cu 2p region for an "*as prepared*" and an "*aged*" sample of **Cu(OAc)$_2$-TS-SILLP-5a**, which is solely exposed to air and light but not to any reactants (Fig. S2c†). The Cu 2p$_{3/2}$ peak, located at a binding energy of 933.3 eV, corresponds to the Cu(I) oxidation state.[31] Meanwhile, the peak found at 935.6 eV is attributed to the Cu(II) state. Peaks observed around 941.6 eV in the Cu 2p$_{3/2}$ region, are the result of a shake-up process linked to the open 3d^9 electron shell configuration of Cu(II). Taking this into account, the XPS analysis reveals the presence of mixed-valence states of copper(I,II)

in the "*as-prepared*" **Cu(OAc)$_2$-TS-SILLP-5a** catalyst, with a shift towards a predominance of copper(I) in the "aged" catalyst (Fig. S2c†). The satellite peaks observed at 941.6 and 941.3 eV in the "*as-prepared*" catalyst, respectively, are characteristic of oxidized Cu(II) sites,[32] commonly seen in the 938–945 eV range (Fig. S2c†).

Notably, the area under these peaks decreases significantly, from 3.3% in the as-prepared material to 0% in the aged material, indicating a decrease in the oxidized Cu(II) sites (Fig. S2c and Tables S3, 4†). The absence of indicators for copper hydroxide, copper acetate, or a copper carbene complex in the XPS data – where the Cu $2p_{3/2}$ peak for copper acetate would be around 934.0 eV, for copper hydroxide between 934.5 and 935.0 eV, and for a copper carbene complex around 936.0 eV – further supports these findings. Regarding the peaks derived from S–H, S $2p_{1/2}$, and S $2p_{3/2}$ of the S–C bonds observed in the S 2p spectra (155–177 eV), significant changes were observed for the "*as prepared*" and the "*aged*" samples. Peaks derived from reduced S–H (S^{2-}) are observed in the 162–165 eV region of the S 2p spectra (S $2p_{3/2}$),[33] while a peak derived from disulfide bonds S–S appears at a binding energy of 166–167 eV.[33,34] XPS analyses confirm the formation of copper–thiol complexes since two S 2p doublets and splitting of 1.2 eV are observed in the region 160–166 eV. According to the literature,[32] the peaks at higher energy could be assigned to free thiols while those at lower energy are characteristic of bound thiolate species. However, one cannot rule out that the electron donation from the sulfur atom of the thiol group to the electrophilic copper site could increase the binding energy of the resulting metal thiolate complexes. These reduced sulfhydryl S^{2-} signals decrease with reuse, while the signal associated with disulfide bonds S–S (S_2^{2-}) at 166–167 eV increased from 5.4% to 20.4% for the "*as prepared*" and the "*spent*" sample, respectively (refer to Fig. S4, Fig. S5 and Tables S5, 6†), which can be related with the thiol assisted reduction of Cu(II) to Cu(I).

The Cu(I) species within these catalysts are inherently unstable, and are prone to easy oxidation back to Cu(II) or undergo disproportionation to form Cu(0) and Cu(II). This instability, in the absence of a regeneration protocol, limits the stability of the catalyst upon reuse (Fig. 3A). This can be appreciated in the XPS spectra of the Cu 2p region of the spent catalyst, **Cu(OAc)$_2$-TS-SILLP-5a**, after five reaction cycles (Fig. S4a†). The spectra reveal the complete absence of the satellite shake-up peaks at 941.6 and 962.3 eV associated with Cu^{2+} species. Although the difference between Cu(0) and Cu(I) XPS spectra is subtle, and assuming the absence of Cu^{2+} species due to the lack of satellite shake-up peaks, the ratio of Cu(I)/Cu(0) components – whether related to CuNPs, complex Cu(I), or Cu_2O – varies with reuse, leading to the formation of reduced Cu species, justifying the loss of activity upon reuse. Table S3† indicates such reduction in the copper oxidation state since the binding energies of the Cu signals decrease from 933.3/953.0 eV (for the "as prepared" sample) to 933.1/952.8 eV (for the "aged" sample) and 932.5/952.3 eV (for the "spent" sample).

In the multicatalytic system **RB-Cu(OAc)$_2$-TS-SILLP-5a**, the Rose Bengal (RB) dye serves as the regeneration agent. This dye, upon electronic excitation by ultraviolet light at a specified wavelength (551 nm), undergoes intersystem crossing (ISC) to reach its excited triplet state, ^{3}RB*, which plays a crucial role in the regeneration process.[35,36] This excited state of RB facilitates the conversion of Cu(I) and Cu(0) back to Cu(II), thereby enabling the reactivation of the catalyst. The regeneration proceeds *via* two potential pathways from the ^{3}RB*state: either through reductive quenching, leading to $RB^{\bullet-}$, or *via* oxidative quenching, resulting in $RB^{\bullet+}$, as illustrated in cycle (a) and cycle (b) of Fig. 5, respectively.

Like the copper–cysteine interactions observed in enzymatic systems, the ^{3}RB* state can donate an electron, promoting the reductive cleavage of the oxidized TSSIL–S–S–TSSIL bond, thereby generating two free thiol groups. In this process, $RB^{\bullet+}$ facilitates the oxidation of Cu(I) back to Cu(II). In the reductive quenching cycle, the amine in the TS-SILLPs, TEA, may act as an electron donor in the presence of ^{3}RB*, leading to the formation of $RB^{\bullet-}$. This radical can then reduce dissolved oxygen to generate superoxide ($O_2^{\bullet-}$) and subsequently hydrogen peroxide (H_2O_2). Both $O_2^{\bullet-}$ and H_2O_2 can promote the conversion of Cu(0) and Cu(I) back to Cu(II) species.

Following a reactivation cycle, the area of the satellite shake-up the peaks at 941.6 and 962.3 eV associated with Cu^{2+} species increases from 0% in the "*spent*" **Cu(OAc)$_2$-TS-SILLP-5a** catalyst (Fig. S4(a) *vs.* (c)†) to 5.8% in the "*regenerated*" one. Additionally, the distribution of the other peaks at 933.9 and 935.6 eV or 953 and 954.9 eV in the "*regenerated*" catalyst shows a similar profile and distribution as in the "*as prepared*" catalyst. Indeed, the binding energy increases from 933.1/952.8 eV (for the "spent" sample) to 933.8/953.5 eV (for the "regenerated" sample), pointing to the oxidation of the reduced copper sites of the "spent" sample. This suggests that the initially present Cu(II) sites are regenerated upon irradiation. These changes in the copper state can also be observed by UV diffuse reflectance spectroscopy of the "*regenerated*" catalyst (Fig. S6†). After use and regeneration, the catalyst shows, in addition to the bands assignable to RB at approximately 519 nm and 562 nm, two additional bands assignable S–Cu(II) charge transfers, appearing at approximately 670 nm and 700 nm.[37]

In the sulfur 2p (S 2p) spectra, peaks deriving from S–H groups are observed in the 162–164 eV range, with an area of 7.7% for the as-prepared material and 6.4% for the "*spent*" catalyst. However, for **RB-Cu(OAc)$_2$-TS-SILLP-5a** after reactivation induced by the photocatalytic treatment, the peak area increases from 6.4% to 9.3%, indicating an increase in the presence of S–H groups (Tables S5 and 6†). Similarly, peaks corresponding to disulfide (S–S) bonds, which appear at a binding energy of 166–167 eV,[24,33] show a slightly higher area of 11.1% in the regenerated catalysts, compared to approximately 20% in the "*spent*" **Cu(OAc)$_2$-TS-SILLP-5a** catalyst after five uses (Fig. S4 and S5 and Tables S5 and S6†). This decrease in area demonstrates changes in sulfur species during the catalytic and reactivation processes. It reveals the key role played by the thiol groups during both reaction and regeneration processes.

Thus, reactivation with RB, *via* either the oxidative or reductive pathway, can restore the copper species activity required for the next catalytic cycle. Importantly, RB does not affect the typical progression of the CuAAC reaction since this reaction is carried out in the absence of oxygen and ultraviolet light, ensuring that the catalytic activity remains unaffected by the presence of RB during the reaction phase.

Evaluation of the environmental impact

The environmental impact of the prepared catalyst was systematically compared with other processes reported in the literature for the synthesis of Rufinamide. Chanda and colleagues provided a comprehensive review of various synthetic routes for Rufinamide, offering a valuable benchmark for evaluating the environmental performance of alternative methods.[38] In this study, the environmental efficiency of the **$Cu(OAc)_2$-TS-SILLP-5a** catalyst was assessed using the *E*-factor, a widely recognized metric for quantifying waste generation in chemical processes (Table S9†). Compared to the conventional use of $Cu(OAc)_2$, which has an *E*-factor of 98, the **$Cu(OAc)_2$-TS-SILLP-5a** system reduced the *E*-factor to 21 (entries 1 *vs.* 2, Table S9†). This substantial reduction underscores the greener nature of our catalyst, as it significantly minimizes waste in Rufinamide synthesis. Furthermore, when compared with three other synthetic routes for Rufinamide, our catalytic system demonstrated a reduction in the *E*-factor, with decreases of up to 83%, or approximately 65%, depending on the reference process (Table S9†). These results highlight the environmental advantages of **$Cu(OAc)_2$-TS-SILLP-5a**, making it a more sustainable option for Rufinamide production compared to established methods in the literature.

Conclusions

In conclusion, this study introduces a groundbreaking approach to enhancing the efficiency and sustainability of copper-catalyzed reactions through the development of task-specific support ionic liquid-like phases. The multifaceted roles of TS-SILLPs are central to overcoming the inherent challenges faced by traditional ionic liquids and copper catalysts. Firstly, the TS-SILLPs offer an effective platform for stabilizing copper ions, particularly the Cu(I) state, crucial for the catalytic activity in reactions such as the [3 + 2] cycloaddition to form triazoles. This stabilization prevents the premature oxidation of Cu(I) to Cu(II), thereby enhancing the effectiveness of the catalyst and the reaction rate.

Secondly, the ionic units within TS-SILLPs act as scavengers for charged and nanoparticle species, significantly minimizing the leaching of metal into the reaction mixture. This feature ensures the heterogeneous nature of the catalyst and the purity of the reaction products, which is particularly valuable in pharmaceuticals and fine chemicals where contamination by catalyst components is a concern.

Moreover, the incorporation of nitrogen-type ligands and free thiol groups in the TS-SILLPs mirrors strategies found in nature, where such functional groups stabilize metal ions and facilitate redox reactions. These ligands protect the copper ions from degradation, thereby extending the lifespan of the catalyst and improving the overall efficiency of the catalytic process.

Finally, the inclusion of a photosensitizer like Rose Bengal within the TS-SILLP framework addresses the challenge of catalyst deactivation through an innovative regeneration mechanism. This mechanism ensures the reactivation of the copper species, allowing for multiple cycles of use without significant loss of activity. The ability of SILLPs to host and activate photosensitizers underscores their versatility and potential for facilitating the recovery of active copper species, thus enhancing the longevity of the catalyst.

This study explores the strategic functionalization of SILLPs with task-specific motifs. The successful implementation of SILLPs in copper-catalyzed azide–alkyne cycloaddition reactions demonstrates their significant advantage over conventional catalysts, offering a versatile and sustainable solution to the challenges of modern catalysis.

Author contributions

Conceptualization by RP and EGV; experimental methodology and analysis by SA, RP, NM, BA, FGC and EGV; experimental work by SA and RP; writing – original draft by RP, NM, FGC and EGV; writing – review & editing by all authors; supervision by RP and EGV; project administration by FGC, NM, BA and EGV; funding acquisition by FGC, NM, BA and EGV.

Data availability

All the data supporting this article have been included as part of the ESI.†

The data were treated with OriginPro and the NMR data were treated with Mestre lab Mnova software suite to process analytical chemistry data.

Conflicts of interest

There are no conflicts to declare.

Acknowledgements

FGC and NM acknowledge the "Ramon y Cajal" contract with code RYC2020-028681-I and RYC2021-033167-I funded by MCIN/AEI/10.13039/501100011033 and by "ESF investing in your future", "European Union NextGenerationEU/PRTR". This work has been partially supported by MICINN-FEDER-AEI 10.13039/501100011033 (PID2021-124695OB-C22, PID2022-142897OA-I00), MCIN/AEI/10.13039/501100011033 and by the European Union Next Generation EU-PRTR (TED2021-

129626B-I00 and TED2021-130288B-I00). FGC thanks Generalitat Valenciana (CISEJI/2023/78).

References

1 J. Dupont, B. C. Lea, P. Lozano, A. L. Monteiro, P. Migowski and J. D. Scholten, *Chem. Rev.*, 2024, **124**, 5227–5420.
2 S. Montolio, B. Altava, E. García-Verdugo and S. V. Luis, Supported ILs and Materials Based on ILs for the Development of Green Synthetic Processes and Procedures, in *Green Synthetic Processes and Procedures*, R. Royal Society of Chemistry, Green Chemistry Series, 2019.
3 A. Mirjafari, *Chem. Commun.*, 2018, **54**, 2944–2961.
4 D. Obrecht and J. M. Villalgordo, Solid-Supported Combinatorial and Parallel Synthesis of Small-Molecular-Weight Compound Libraries, in *Tetrahedron Organic Chemistry Series*, 1998.
5 H. C. Kolb, M. G. Finn and K. B. Sharpless, *Angew. Chem., Int. Ed.*, 2001, **40**, 2004–2021.
6 C. W. Torne, C. Christensen and M. Meldal, *J. Org. Chem.*, 2002, **67**, 3057–3064.
7 V. V. Rostovtsev, L. G. Green, V. V. Fokin and K. B. Sharpless, *Angew. Chem., Int. Ed.*, 2002, **41**, 2596–2599.
8 E. Bonandi, M. S. Christodoulou, G. Fumagalli, D. Perdicchia, G. Rastelli and D. Passarella, *Drug Discovery Today*, 2017, **22**, 1572–1581.
9 R. Varala, H. B. Bollikolla and C. M. Kurmarayun, *Curr. Org. Synth.*, 2021, **18**, 101–124.
10 L.-S. Feng, M.-J. Zheng, F. Zhao and D. Liu, *Arch. Pharm.*, 2021, **354**, e2000163.
11 D. R. Buckle, C. J. M. Rockell, H. Smith and B. A. Spicer, *J. Med. Chem.*, 1984, **27**, 223–227.
12 N. G. Aher, V. S. Pore, N. N. Mishra, A. Kumar, P. K. Shukla and A. Sharma, *Bioorg. Med. Chem. Lett.*, 2009, **19**, 759–763.
13 Z. Xu, S.-J. Zhao and Y. Liu, *Eur. J. Med. Chem.*, 2019, **183**, 111700.
14 Y. Cao and H. Lu, *Future Med. Chem.*, 2021, **13**, 2107–2124.
15 A. Pathigoolla, R. P. Pola and K. M. Sureshan, *Appl. Catal., A*, 2013, **453**, 151–158.
16 B. Dervaux and F. E. Du Prez, *Chem. Sci.*, 2012, **3**, 959–966.
17 P. Veerakumar, N. Velusamy, P. Thanasekaran, K.-C. Lin and S. Rajagopal, *React. Chem. Eng.*, 2022, **7**, 1891–1920.
18 S. Chassaing, V. Bénéteau and P. Pale, *Catal. Sci. Technol.*, 2016, **6**, 923–957.
19 A. Kumar, V. Kumar, P. Singh, R. K. Tittal and K. Lal, *Green Chem.*, 2024, **26**, 3565–3594.
20 M. K. Muthyala, K. Velisetti, K. Parang and A. Kumar, *Curr. Org. Chem.*, 2014, **18**, 2530–2554.
21 S. I. Presolski, V. Hong, S.-H. Cho and M. G. Finn, *J. Am. Chem. Soc.*, 2010, **132**, 14570–14576.
22 M. Prudent and H. H. Girault, *Metallomics*, 2009, **1**, 157–165.
23 A. V. Kachur, C. J. Koch and J. E. Biaglow, *Free Radic. Res.*, 1998, **31**, 23–34.
24 J. Rull-Barrull, M. d'Halluin, E. Le Grognec and F.-X. Felpin, *Angew. Chem.*, 2016, **128**, 13747–13750.
25 A. Selim, K. M. Neethu, V. Gowri, S. Sartaliya, S. Kaur and G. Jayamurugan, *Asian J. Org. Chem.*, 2021, **10**, 3428–3433.
26 D. Bermejo-Velasco, A. Azémar, O. P. Oommen, J. Hilborn and O. P. Varghese, *Biomacromolecules*, 2019, **20**, 1412–1420.
27 G.-C. Kuang, P. M. Guha, W. S. Brotherton, J. T. Simmons, L. A. Stankee, B. T. Nguyen, R. J. Clark and L. Zhu, *J. Am. Chem. Soc.*, 2011, **133**, 13984–14001.
28 B. Wang, J. Durantini, J. Nie, A. E. Lanterna and J. C. Scaiano, *J. Am. Chem. Soc.*, 2016, **138**, 13127–13130.
29 D. Valverde, R. Porcar, P. Lozano, E. García-Verdugo and S. V. Luis, *ACS Sustainable Chem. Eng.*, 2021, **9**, 2309–2318.
30 B. K. Maiti, L. B. Maia, A. J. Moro, J. C. Lima, C. M. Cordas, I. Moura and J. J. G. Moura, *Inorg. Chem.*, 2018, **57**, 8078–8088.
31 M. Swadźba-Kwaśny, L. Chancelier, S. Ng, H. G. Manyar and C. Hardacre, *Dalton Trans.*, 2012, **41**, 219–227.
32 J. Rull-Barrull, M. d'Halluin, E. Le Grogneca and F.-X. Felpin, *Chem. Commun.*, 2016, **52**, 6569–6572.
33 H. Mekaru, A. Yoshigoe, M. Nakamura, T. Douraand and F. Tamanoi, *ACS Appl. Nano Mater.*, 2019, **2**, 479–488.
34 P. Zhang, N. Zhang, Q. Wang, P. Wang, J. Yuan, J. Shen and X. Fan, *Carbohydr. Polym.*, 2019, **203**, 369–377.
35 G. Szczepaniak, J. Jeong, K. Kapil, S. Dadashi-Silab, S. S. Yerneni, P. Ratajczyk, S. Lathwal, D. J. Schild, S. R. Das and K. Matyjaszewski, *Chem. Sci.*, 2022, **13**, 11540–11550.
36 H. I. Coskun, F. De Luca Bossa, X. Hu, S. Jockusch, J. Sobieski, G. Yilmaz and K. Matyjaszewski, *J. Am. Chem. Soc.*, 2024, **146**, 28994–29005.
37 J.-Y. Jung, M. Kang, J. Chun, J. Lee, J. Kim, J. Kim, Y. Kim, S.-J. Kim, C. Lee and J. Yoon, *Chem. Commun.*, 2013, **49**, 176–178.
38 R. D. Padmaja and K. Chanda, *Org. Process Res. Dev.*, 2018, **22**, 457–466.

